Complex Oxygen Regimes of Water Objects Under the Anthropogenic Loading

Inna Skurativska, Sergii Skurativskyi, Oleksandr Popov, Deineka Viktoriia, Eduard Mykhliuk, and Maksym Dement

Abstract Under conditions of intense anthropogenic loading in combination with climate change, the significant degradation of water resources of the planet, especially surface waters, is observed. The surface waters are the environment where a vast part of natural ecosystems dwell, and provide the major source of drinking water. They are also an extremely important element of technological processes in industry, agriculture, and etc. Therefore, the assessment, control, and forecasting of surface water quality are in a focus of many scientific investigations. This report deals with the oxygen regime of water objects (basins of self-purification) which is studied by the methods of mathematical modeling. The oxygen regime description consists of the balance equations governing the dynamics of oxygen, i.e. biochemical oxygen demand (BOD) and dissolved oxygen (DO), phosphorus, and phytoplankton. The resulting nonlinear dynamical system is studied by the numerical and qualitative analysis methods. It is shown that the model possesses the steady solutions in a vicinity of which the nonlinear periodic regimes can occur. When the parameters of nonlinearity vary, the periodic regimes lose their stability and multiperiodic regimes appear. Among complex system's solutions, there are also chaotic regimes. Furthermore, we developed the model for the river system which consists of coupled dynamical systems describing the bio-chemical processes in two connecting self-purificating basins. This model possesses the nonlinear periodic regimes as well.

I. Skurativska (✉) · S. Skurativskyi
Subbotin Institute of Geophysics of NAS of Ukraine, Kyiv, Ukraine

S. Skurativskyi · O. Popov
State Institution, The Institute of Environmental Geochemistry of National Academy of Sciences of Ukraine, Kyiv, Ukraine

O. Popov
Pukhov Institute for Modelling in Energy Engineering of NAS of Ukraine, Kyiv, Ukraine

Interregional Academy of Personnel Management, Kyiv, Ukraine

D. Viktoriia · E. Mykhliuk · M. Dement
National University of Civil Defence of Ukraine, Kharkiv, Ukraine

A. Zaporozhets (ed.), *Systems, Decision and Control in Energy III*,
Studies in Systems, Decision and Control 399,
https://doi.org/10.1007/978-3-030-87675-3_20

Keywords Modified Streeter–Phelps equation · Water pollution · Basin of self-purification · Nonlinear dynamical systems · Bifurcations · Chaos

1 Introduction

Water is a good solvent and can transport substances which adversely affect biological systems, including human health, over long distances through river systems. Due to its geographical (geological, relief) location, water objects are the endpoint of the waste water accumulation of the most of man-made substances formed in a catchment area. At the same time, natural waters are in constant circulation and actively interact with the main components of the biosphere, atmosphere, lithosphere, aquatic, and terrestrial ecosystems [1–3]. Therefore, hydro-ecological features of surface water quality serve the natural indicator of ecological welfare of both aquatic ecosystems and the entire catchment area [4]. Since surface runoff is formed in the catchment area, where different pollution sources (agricultural complexes, industrial facilities, mining facilities [5]) are located, it becomes obvious that to assess water quality [6–8] we should quantify the impact of these facilities, find out the nature of pollution and ways to overcome the negative impact of polluting components (involving natural factors) on the ecosystem's elements.

Determining the oxygen regime of surface waters is an important component of assessing the state of aquatic ecosystems and catchment areas. Dissolved oxygen ensures the viability of living organisms and the self-purificating function of the aquatic ecosystem. The participation of oxygen in the processes of biological, chemical and physical–mechanical self-purification of water objects indicates that the assessment of the concentration of dissolved oxygen is of great practical and general scientific importance [9, 10]. Taking into account the complexity of conducting a series of ecological experiments, the synergy of ecosystem components [11, 12], the lack of comprehensive information about their interaction, the tasks of estimating, predicting, and controlling the oxygen regime using mathematical modeling remain insufficiently studied [13–18]. Especially this concerns the phenomena of self-organization inherent in ecosystems. To take into account the nonlinear and cooperative effects [19, 20], we generalize our previous investigations [13–18] of the processes of oxygen regime formation. Therefore, the purpose of these studies is to classify the nonlinear oxygen regimes that can be observed in the target system and to establish their bifurcations.

2 Mathematical Model for the Oxygen Regime Description

The surface water quality [21] of a water object is characterized by the oxygen dynamics, which in turn essentially depends on different biogenic elements (here we consider the phosphorus dynamics) and the phytoplankton behavior [4, 19]. In

particular, the oxygen transformations are characterized by the biochemical oxygen demand (BOD) representing the indicator of the total organic content reacting with oxygen [22, 23] and dissolved oxygen (DO), i.e. amount of oxygen containing in water [24]. For modeling BOD and DO dynamics, it is known the Streeter and Phelps model [6, 7] and its modifications [6, 22, 25–27]. These models are mostly linear with large number of parameters and do not take into account accompanied processes affecting the oxygen regime.

Therefore, to develop the mathematical model describing the dynamics of the quantities BOD, DO, phytoplankton, and phosphorus, we construct the balance equations for the corresponding concentrations C_{BOD}, C_{DO}, C_{PhT} and C_P.

At first, consider the processes governing the incoming and outcoming oxygen fluxes. Sources of oxygen supply primarily include: re-aeration (invasion), i.e. saturation (enrichment) of water with oxygen; oxygen supply with external water flows from a catchment area; oxygen replenishment due to photosynthesis of algae and higher aquatic plants.

Oxygen consumption items that cannot be neglected in the analysis of the oxygen regime of aquatic environment include evasion, i.e. the process of oxygen transfer from water to air and is based on the same physical principles as the invasion process; destruction of organic compounds (respiration of microorganisms); oxidation of inorganic compounds with the formation of oxides, such as the process of nitrification, the spending on respiration of aquatic organisms.

Closely related to the dynamics of BOD and DO is the phenomenon of reservoir eutrophication representing the water enrichment with nutrients (mainly phosphorus and nitrogen), which cause the growth of primary organic matter production due to intensification of metabolic processes in algae and higher aquatic vegetation. The main indications of reservoir eutrophication are the predominance of production processes over destructive, which is accompanied by a significant increase in nutrients. This phenomenon, in turn, provokes the growth of biomass of phytoplankton, phytobenthos, filamentous algae to the level of water "blooming", reducing the concentration of dissolved oxygen.

On the one hand, the growth of phytoplankton biomass is a positive phenomenon because the forage base for aquatic organisms and oxygen level increase. However, there comes a moment when the balance between the growth of algal biomass, the formation of organic matter, oxygen and destructive processes is disturbed. Ultimately, the physicochemical properties of the environment change: the level of nutrients and organic matter increases, the level of dissolved oxygen decreases, anaerobic zones appear and expand, turbidity increases and water transparency decreases, and so on. As a result of the activity of algae and their decomposition, the oxygen content in the water decreases and the concentration of toxic substances increases, which causes mass death of fish and invertebrates [4]. However, the process of reservoir eutrophication is determined not only by the accumulation of nutrients, but also by the degree of water exchange, the reservoir depth and volume, and the oxygen saturation degree. Therefore, the process of eutrophication is considered as a result of the interaction of biotic and abiotic factors, which gives it an ecosystem character,

and its study requires a systematic approach and the use of methods of mathematical modeling.

Thus, the resulting mathematical model for the oxygen regime dynamics reads as follows:

$$\begin{aligned}
\frac{dC_{BOD}}{dt} &= \frac{Q_{BOD}}{W} - \left[k_1(C_{DO}) + \frac{q}{W}\right]C_{BOD} + m_1 C_{PhT} - \lambda C_{BOD} C_{DO} \\
\frac{dC_{DO}}{dt} &= \frac{Q_{DO}}{W} + k_2 C^* + \alpha C_{PhT} - \left[k_2 + \frac{q}{W}\right]C_{DO} - k_1(C_{DO}) C_{BOD} \\
\frac{dC_{PhT}}{dt} &= \frac{Q_{PhT}}{W} + [k_3(C_{DO}, C_P) - m]C_{PhT}, \\
\frac{dC_P}{dt} &= \frac{Q_P}{W} - n_1 C_{PhT} + n_2 C_{BOD} - \frac{q}{W} C_P,
\end{aligned} \tag{1}$$

where Q_{BOD}, Q_{DO}, Q_{PhT}, and Q_P denote rates of addition of corresponding component from the outside; W is the volume of water object; q stands for the incoming flow; C^* is the oxygen concentration at its saturation; the function $k_1(C_{DO})$ is the rate for oxygen consumption by BOD; k_2 is the aeration coefficient; the function $k_3(C_{DO}, C_P)$ and m are the rate of phytoplankton growth and death, respectively; $m_1 = \gamma m$, γ stands for the fraction of dead phytoplankton for oxidation;αC_{PhT} is the rate of oxygen adding during photosynthesis;λ is the coefficient of non-conservativity at the nonlinear interaction of organic substance and oxygen; n_1 is the rate of phosphorus depletion due to phytoplankton; n_2 is the rate of phosphorus production from organic substance (detritus).

To identify the functions $k_1(C_{DO})$ and $k_3(C_{DO}, C_P)$, the Michaelis–Menten kinetics [6, 28] is used. In particular,

$$k_1(C_{DO}) = k_1 \frac{C_{DO}}{K_{DO} + C_{DO}} \text{and} \, k_3(C_{DO}, C_P) = k_3 \frac{C_{DO}^n}{K_\nu^n + C_{DO}^n} \cdot \frac{C_P}{K_\mu + C_P}.$$

Here the parameters k_1 and k_3 are the constants of saturation defining the behavior of functions at infinity, n is an empirical paramet88er. The parameters K_{DO}, K_ν, and K_μ stand for the half saturation constants.

It should be noted that system (1) can be regarded as a generalization of the well-known Streeter–Phelps equations for the assessment of water quality [6, 7, 27, 29].

Next, let us write system (1) in dimensionless form applying the scale transformation

$$\{C_{BOD}; C_{DO}; C_{PhT}; C_P\} = \langle C_{DO} \rangle \{x; y; z; u\},$$

where $\langle C_{DO} \rangle$ is a charactristic value of DO concentration; *x, y, z, u* are the dimensionless quantities.

Thus, utilizing the notatins

$$\frac{Q_{BOD}}{W\langle C_{DO}\rangle} = A,\ \frac{1}{\langle C_{DO}\rangle}\left(\frac{Q_{DO}}{W} + k_2 C^*\right) = B,\ \frac{Q_{PhT}}{W\langle C_{DO}\rangle} = F,\ \frac{Q_P}{W\langle C_{DO}\rangle} = C$$
$$\frac{q}{W} = S,\ \lambda\langle C_{DO}\rangle = \overline{\lambda},\ \frac{K_{DO}}{\langle C_{DO}\rangle} = \overline{K}_{DO},\ \frac{K_v}{\langle C_{DO}\rangle} = \overline{K}_v,\ \frac{K_\mu}{\langle C_{DO}\rangle} = \overline{K}_\mu,$$

and dropping the bar over the symbols, the final form of dynamical system is as follows:

$$\begin{aligned}
\frac{dx}{dt} &= A - \left[\frac{k_1 y}{K_{BOD} + y} + S\right]x + m_1 z - \lambda x y,\\
\frac{dy}{dt} &= B + \alpha z - [k_2 + S]y - \frac{k_1 y}{K_{BOD} + y}x,\\
\frac{dz}{dt} &= F + \left[k_3 \frac{y^n}{K_v^n + y^n} \cdot \frac{u}{K_\mu + u} - m\right]z,\\
\frac{du}{dt} &= C - n_1 z + n_2 x - S u.
\end{aligned} \tag{2}$$

Now we are going to consider the solutions of autonomous system (2) using the qualitative analysis method [30]. According to the method, at first, the fixed points of system (2) should be derived. Then the stability of these points is considered in the linear approximation. In particular, we are interested in the conditions of lose of stability for the fixed points. These conditions provide the constraints for the model's parameters at which the development of nonlinear periodic solutions (limit cycle) can be possible. To validate the limit cycle appearance, the direct numerical integration of system (2) is used.

3 Stationary Solutions of the Mathematical Model Describing the Oxygen Regime

Thus, the fixed points of system (2) representing the steady oxygen regimes in water objects satisfy the nonlinear algebraic system

$$\begin{aligned}
&A - \left[\frac{k_1 y}{K_{BOD} + y} + S\right]x + m_1 z - \lambda x y = 0,\\
&B + \alpha z - [k_2 + S]y - \frac{k_1 y}{K_{BOD} + y}x = 0,\\
&F + \left[k_3 \frac{y^n}{K_v^n + y^n} \cdot \frac{u}{K_\mu + u} - m\right]z = 0,\\
&C - n_1 z + n_2 x - S u = 0.
\end{aligned} \tag{3}$$

To get solutions of this nonlinear system, the iterational numerical Newton's process is used. In the matrix form, the numerical procedure is described by the sequence:

$$X_{p+1} = X_p - J^{-1}(X_p)G(X_p),\ p = 1, 2, \ldots,$$

where J^{-1} is the inverse matrix for the matrix of linearization [31]

$$J = \begin{pmatrix} -\left(S + \lambda y + \frac{k_1 y}{K_{BOD}+y}\right) & -\left(\lambda x + \frac{K_{BOD}k_1 x}{(K_{BOD}+y)^2}\right) & m_1 & 0 \\ -\frac{k_1 y}{K_{BOD}+y} & -\left(S + k_2 + \frac{K_{BOD}k_1 x}{(K_{BOD}+y)^2}\right) & \alpha & 0 \\ 0 & \frac{nk_3 K_v^n u y^{n-1} z}{(K_\mu+u)(K_v^n+y^n)^2} & J_{33} & J_{34} \\ n_2 & 0 & -n_1 & -S \end{pmatrix} \tag{4}$$

Here

$$J_{33} = -m + \frac{k_3 u y^n}{(K_\mu + u)(K_v^n + y^n)},\ J_{34} = \frac{K_\mu k_3 z y^n}{(K_\mu + u)^2 (K_v^n + y^n)}.$$

Using Newton's procedure, let us consider the dependence of coordinates of fixed points on the model's parameter variation. Taking into account that the nonlinearity is related with the variable y while other variables are incorporated into system (2) linearly, the steady solutions is useful to study via the method of parameter mapping [30]. To do this, from the first and the last equations of system (3) we get the following expressions:

$$x = a_1 + a_2 z,\ u = b_1 + b_2 z,$$

where

$$a_1 = \frac{(K_\mu + y)A}{K_\mu(S + \lambda y) + y(k_1 + S + \lambda y)},\ a_2 = \frac{(K_\mu + y)m_1}{K_\mu(S + \lambda y) + y(k_1 + S + \lambda y)}$$
$$b_1 = \frac{C + n_2 a_1}{S},\ b_2 = \frac{n_2 a_2 - n_1}{S}.$$

When these expressions are inserted into the third equation of system (3), it is obtained the quadratic equation with respect to z:

$$F(K_v^n + y^n)(K_\mu + u) + (k_3 y^n u - m(K_v^n + y^n)(K_\mu + u))z = 0,$$

or

$$H_1 z^2 + H_2 z + H_3 = 0,$$

where

$$H_1 = b_2\left(k_3 y^n - m\left(K_v^n + y^n\right)\right), H_2 = \left(b_2 F - mK_\mu\right)\left(K_v^n + y^n\right) + b_1\left(k_3 y^n - m\left(K_v^n + y^n\right)\right),$$
$$H_3 = F\left(b_1 + K_\mu\right)\left(K_v^n + y^n\right).$$

Its roots are as follows:

$$z^- = \frac{-H_2 - \sqrt{H_2^2 - 4H_1H_3}}{2H_1}, z^+ = \frac{-H_2 + \sqrt{H_2^2 - 4H_1H_3}}{2H_1}.$$

Note that the right parts of the relations derived depend on the variable y only. Thus, inserting into the second equation of system (3) the expressions for x and z, we lead to the relation with respect to the variable y and the model's parameters. Solving the resulting equation for α, it is easy to get the following expression

$$\alpha = (k_2 + S)\frac{y}{z} + k_1\frac{yx}{(K_{BOD} + y)z} - \frac{B}{z}, \tag{5}$$

where z should be replaced by z^+ or z^- and x is given above. In what follows, we fix the parameter values:

$$\begin{aligned} &A = 0.933, B = 4.974, C = 2, F = 3, k_1 = 1.5, k_2 = 0.7, W = 1,\\ &q = 0.2, n = 0.44, K_{BOD} = 4.3, K_\mu = 1.14, K_v = 0.296, \lambda = 0.7,\\ &k_3 = 4.65, n_1 = 0.65, n_2 = 0.9, m = 2.3, m_1 = 0.45. \end{aligned} \tag{6}$$

Using these parameters, one can depict the function $\alpha(y)$ in Fig. 1, where the profile of $\alpha(y)$ at $z = z^-$ is shown by the solid curve and $\alpha(y)$ at $z = z^+$—by the dashed curve.

From Fig. 1 it follows that, depending on α, we can derive from one to four roots of system (3). In particular, at $\alpha = \alpha_0 = 0.05$ (Fig. 1) there are three points lying in the curve derived at $z = z^-$ and one root belonging to the curve plotted at $z = z^+$. The coordinates of three fixed points now can be evaluated by Newton's method with the accuracy 10^{-5} and then the eigenvalues of the linearized matrix J can be obtained as well.

Thus, the coordinates of

Point I: (123.30026; 0.27971; 131.47888; 137.54482) and corresponding eigenvalues $\xi = (-39.42; 0.031 \pm 0.33i; -0.17)$ of the matrix J at this point. Since there is the complex-valued eigenvalues with positive real parts, the fixed point is an unstable focus.

Point II: (0.54449; 5.22832; 3.59295; 0.77313), the eigenvalues $\xi = (-4.69; -0.56 \pm 1.48i; -0.84)$. Since all real parts of ξ_j are negative, then the fixed point is a stable focus.

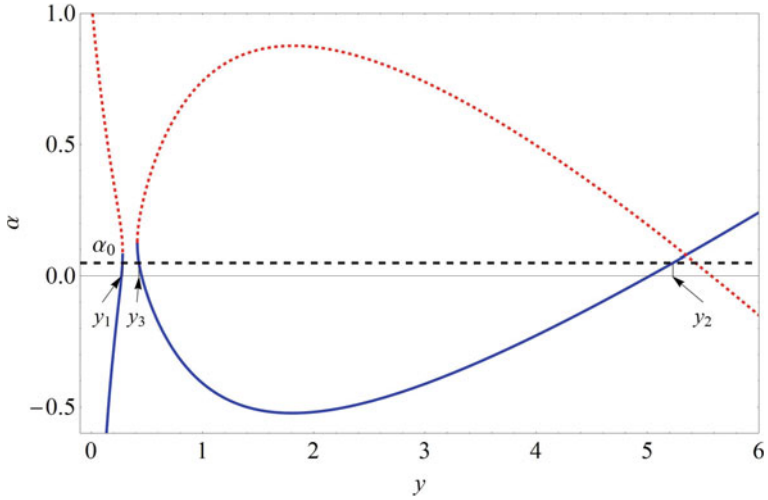

Fig. 1 The graph of function $\alpha(y)$ defined by relation (5). Here y_1, y_2, and y_3 are the y-coordinates of the fixed points I, II, and III, respectively

Point III: (68.77574; 0.42813; 95.05617; 10.55825), the eigenvalues $\xi = (-21.43; -0.16 \pm 1.19i; 0.16)$. Since there is a positive eigenvalue and pair complex-valued ones, then the fixed point is a saddle-focus.

It is worth noting that the dependence $\alpha(y)$ allows one to consider the influence of the parameters of nonlinearity λ and n on the position of the roots of system (3), i.e. the shapes of curves in Fig. 1. In particular, when the parameter n increases, i.e. $n = 0.8 > 0.44$, the curves (Fig. 2a) corresponding to $z = z^+$ are stretched along $O\alpha$. This causes the growth of interval of α, where there is more than one root of system (3).

When the parameter λ decreases from 0.7 to 0.2, the curve corresponding to $z = z^-$ displaces along vertical axes (Fig. 2b).

To get an idea of the complex structure of the phase space, the analysis of the convergence of Newton's method to the solutions of system (3) is carried out. We choose the initial conditions for running iterations of Newton's method from the domain $\Sigma = \{x, u | 0 \le x \le 300, 0 \le u \le 250\}$. Let us restrict the case with $z = z^+$. Then, as a result of finding the solution of system (3), we obtain one of the three possible roots of the system.

Thus, each starting point for Newton's method is uniquely associated with a certain root of system (3), which is denoted by a shade of black (Fig. 3a). The structure of the set of points and enlargement of the selected domain (Fig. 3b) tell us about the fractal nature of the resulting structure.

After derivation of the coordinates of stationary points, the type of fixed point can be found out by studying the eigenvalues of the matrix of the linearized system. The most interesting cases are related to the changes of the point's types. These changes in turn define the bifurcations of the system's phase space. In particular,

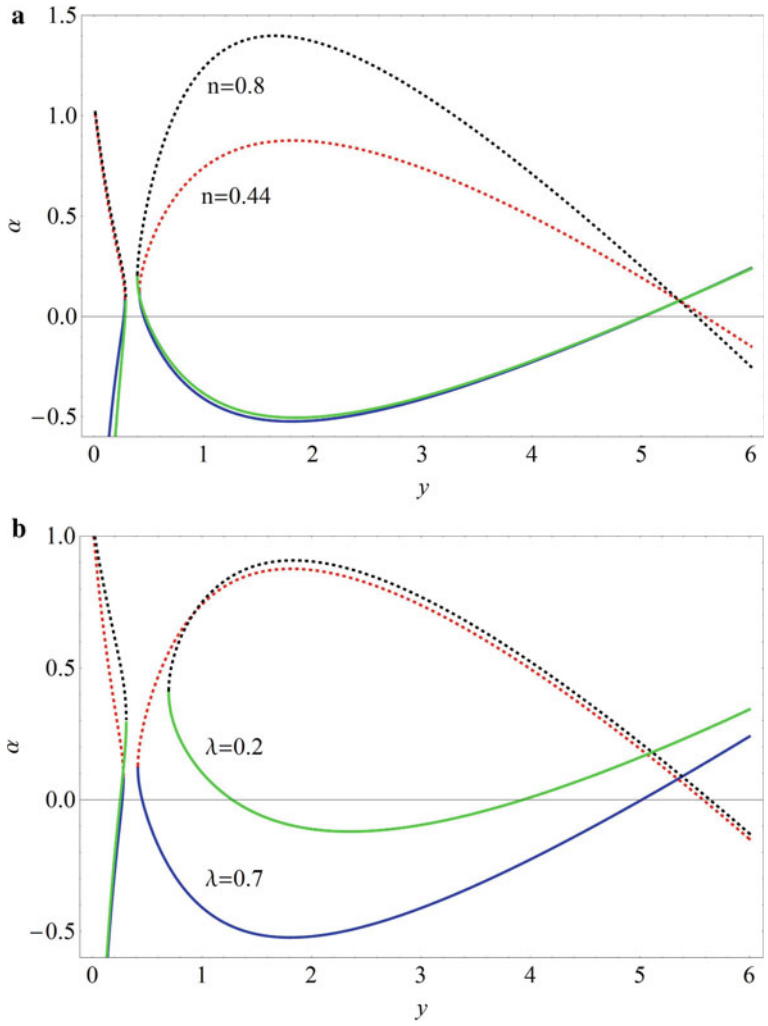

Fig. 2 The positions of roots of system (3) depending on the parameter n (**a**) and the parameter λ (**b**)

we are going to consider the most intriguing case when the real parts of the pair of eigenvalues change their sign from minus to plus. This case is called the Andronov-Hopf bifurcation and corresponds to the birth of a periodic regime in a vicinity of a fixed point.

To identify the Andronov-Hopf bifurcation, we fix the parameter values as above except for the parameter λ. When λ varies, all eigenvalues ρ of the matrix J are evaluated simultaneously with the coordinate of the fixed point I. The resulting dependence of $\mathrm{Re}(\rho)$ on λ is depicted in Fig. 4 (solid curve). From the analysis of

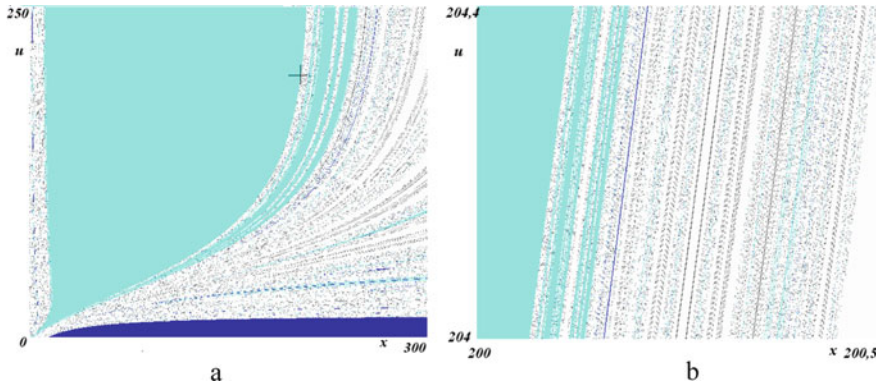

Fig. 3 Diagram of the results of convergence of Newton's method iterations. Shades of black indicate the initial conditions under which Newton's method coincides with one of the three solutions of system (3)

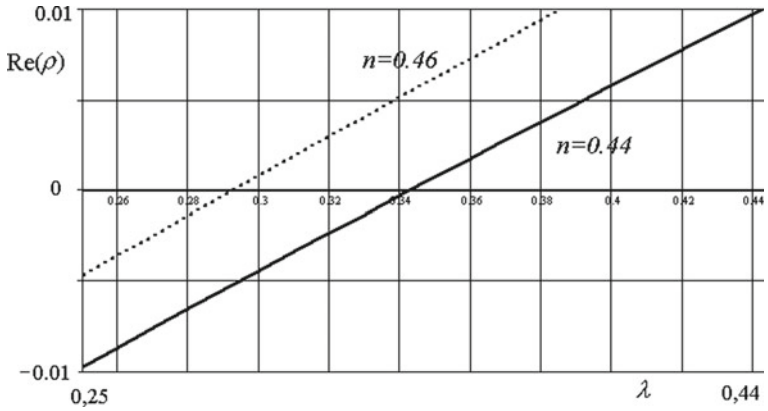

Fig. 4 The dependence of the real part of complex-valued eigenvalues of the matrix J on the parameter λ evaluated for the fixed point I

this figure it follows that at increasing λ the eigenvalue's real part intersects horizontal axes at about 0.34.

It is important to estimate the position of the Andronov-Hopf bifurcation when other parameters vary. In particular, when the parameter of nonlinearity n changes from 0.44 to 0.46, the zero of the function $\mathrm{Re}(\rho)$ moves to the left, i.e. the moment of the periodic regime displaces toward the lower values of λ (dashed curve in Fig. 4).

Thus, if we take λ a little bit larger than 0.34, we can expect to observe the stable limit cycle appearance.

To make sure that periodic oscillations appear, when λ grows after the Andronov-Hopf bifurcation, we perform the numerical integration of system (2) in a vicinity of the fixed point I. It turned out that, indeed, it is observed the oscillations producing the limit cycle in the system's phase space. Moreover, their amplitude increases when λ grows.

4 Periodic and Chaotic Oxygen Regimes

Now we consider the limit cycle development in more detail at the variation of the parameters n and λ. To evaluate the limit cycle, we choose the initial data for the numerical integration of system (2) close to the fixed point I at $n = 0.44$. After omitting the transient processes, the system approaches the periodic regime, the phase portrait's projection of which is depicted in Fig. 5a. When $n = 0.48$, the double period bifurcation occurs and double limit cycle (Fig. 5b) exists. The result of another period doubling bifurcation is shown in Fig. 6a representing the quadruple limit cycle at $n = 0.50$. Finally, at $n = 0.56$ there is a chaotic attractor (Fig. 6b) in the phase space.

To find out the geometric structure of the chaotic attractor, the Poincare section technique can be used. To apply it, we choose the section plane $\Pi : z = 150$ and evaluate the points of intersection of the plane and a trajectory. In particular, at $n = 0.54$ in this plane the set of points forming the localized islands (Fig. 7a) is observed. When $n = 0.56$, the points of intersections form the strip (Fig. 7b) of fractal structure. Such changes in Poincare section structure indicate the occurring of bifurcations in the chaotic attractor during the parameter n variation. The fact that we observed the "shuffled" narrow strip means that the geometric dimension of the chaotic attractor is measured not by an integer but by a fractional number [30].

Using the same technique, it is useful to analyze the bifurcation diagram describing the development of the stable attractors at increasing n. For diagram construction,

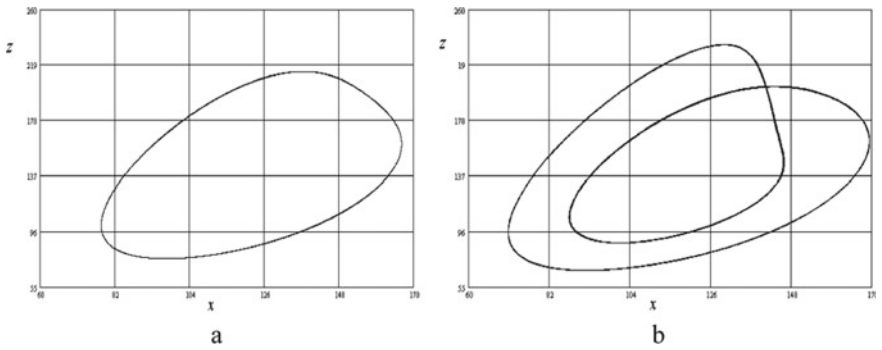

Fig. 5 The projections of the phase portraits on the plane $(x; z)$ of the limit cycles at $n = 0.44$ (**a**) and $n = 0.48$ (**b**)

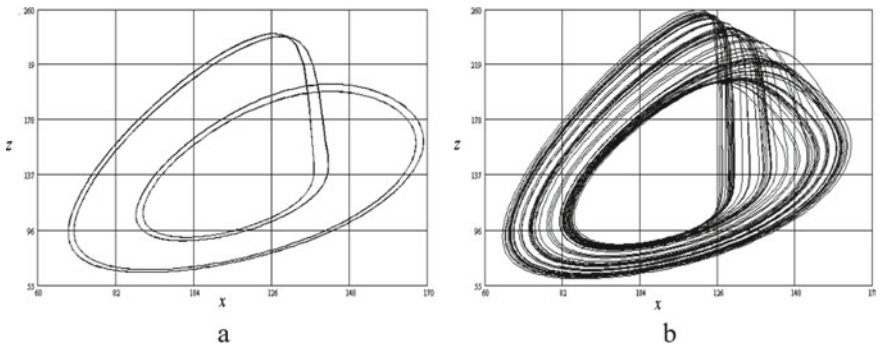

Fig. 6 The phase portraits of the limit cycles at $n = 0.50$ (**a**) and $n = 0.56$ (**b**)

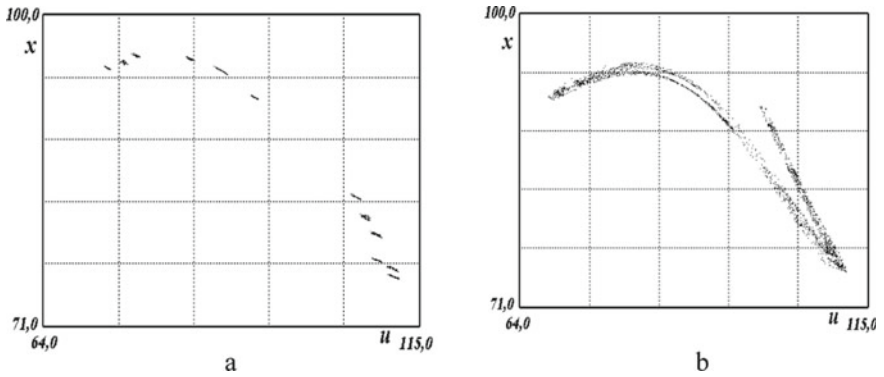

Fig. 7 The Poincare sections of the chaotic attractors existing at $n = 0.54$ (**a**) and $n = 0.56$ (**b**) (here $\lambda = 0.7$)

we put the parameter n along horizontal axes, while the values of x-coordinates of intersection points along vertical one. Thus, we construct the Poincare diagram (Fig. 8a), when $\lambda = 0.7$ and n grows from 0.44, when the limit cycle exists and produces the leftmost point in Fig. 8a, to 0.64 corresponding to another limit cycle existence. This diagram shows the moments of period doubling bifurcations and chaotic attractor development. There is also the separated "window" of solutions with quadruple period. Note that this "window" disappears, when λ increases to 0.72 (Fig. 8b). Instead of the developed chaotic zone, we observe the structure which is inherent to multiperiodic regimes obeying the period-doubling scenario.

In the similar spirit, the Poincare diagrams are constructed at lower λ, i.e. $\lambda = 0.68$ (Fig. 9a) and $\lambda = 0.66$ (Fig. 9b).

Analyzing these diagrams we see that the decreasing λ causes the growth of attractor's size and "window" size too. Moreover, the chaotic zones become more wide and intensive. There is the coexisting chaotic attractor producing the points in the diagrams beyond the main set of points.

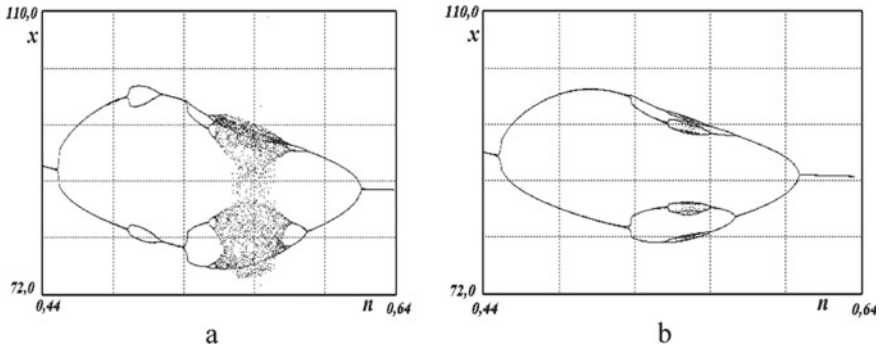

Fig. 8 The Poincare bifurcation diagrams at $\lambda = 0.70$ (**a**) and $\lambda = 0.72$ (**b**), when the parameter n grows

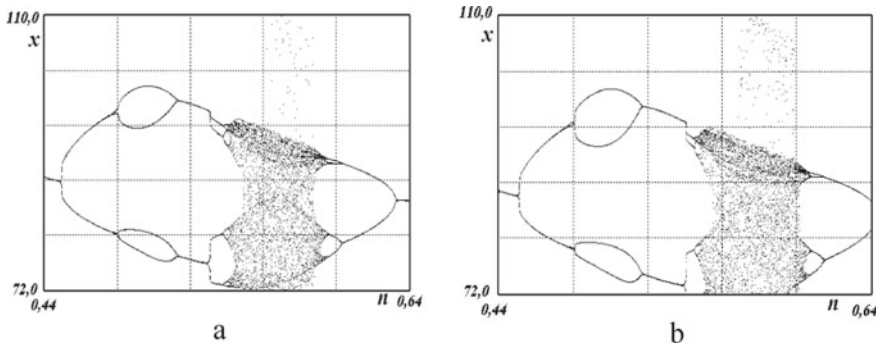

Fig. 9 The Poincare bifurcation diagrams at $\lambda = 0.68$ (**a**) and $\lambda = 0.66$ (**b**) when the parameter n grows

The results of qualitative analysis concerning the periodic regimes can be supplemented by the application of shooting method [30, 32]. According to the method, the initial value problem transforms to the boundary value problem, which is considered over a period of the limit cycle. This method also allows one to evaluate a point lying on the limit cycle with high accuracy, its Floquet multipliers characterizing the limit cycle's stability, and to derive the unstable periodic solutions which are important for understanding the scenarios of bifurcations.

In particular, consider the limit cycle existing at $n = 0.44$ and $\lambda = 0.7$ (Fig. 5a). To realize the shooting method algorithm, the procedures and functions from the "Mathematica" can be used. Thus, starting from the initial data (112.6084; 0.4004; 194.8777; 53.3995) which is close to the limit cycle approximate value of period $T = 17.6$, after application of shooting method we get the refined point's coordinates (112.6084; 0.4003; 194.7685; 53.4728) and limit cycle period $T = 17.5019$. Simultaneously, the Floquet multipliers $\rho_i =$

$(-0.8327;\ 0.9999;\ -0.1398;\ 0)$ are evaluated. Since $|\rho_i| < 1$, we can conclude that the limit cycle considered is stable.

From the Poincare diagram of Fig. 8a it follows that this periodic solution at increasing n is destroyed and instead another periodic regime appears. To find out what happened with the previous regime, we fix $n = 0.45$ and apply the shooting method to the data derived at $n = 0.44$. Then we get the coordinates of cycle's point (112.6084; 0.4037; 197.0695; 51.7384), its period $T = 17.1364$, and the Floquet multipliers $\rho = (-1.0971; 0.9999; -0.1221; 0)$. Since $|\rho_i| > 1$, it means that the derived periodic regime is unstable (repeller). If we take the initial data on the double limit cycle when $T_s = 34.4$, then we obtain the cycle's point (136.2579; 0.2075; 92.5914; 200.5915), its refined period $T_s = 34.2307$, and Floquet multipliers $\rho = (0.9999; 0.6831; 0.0260; 0)$. From the inequality $|\rho_i| < 1$ it follows the stability of the double limit cycle (attractor).

Comparing the periods of stable and unstable limit cycles, we get $T_s/T_u = 1.9558 \approx 2$. From this it follows that we indeed deal with the period doubling bifurcation after which the pair of periodic trajectories coexists.

Thus, we shown that dynamical system (2) possesses the periodic (both stable and unstable) solutions, which undergo the several periodic doubling bifurcations, and chaotic solutions.

5 The Construction of the Mathematical Model for the River System Using the Nonlinear Dynamical Model of the Basin of Self-Purification

One of the possible applications of model (1) is the assessment of oxygen regime for drainage systems. To do this, we assume that the drainage system can be represented by the pair of basins of self-purification. Let these basins join successively. Assume also that the first basin possesses N incoming streams with a rate $q_j, j = 1, ..., N$ each. Then the stream outcoming from the first basin and incoming into the second basin has the rate $\sum_{j=1}^{N} q_j$. The same stream leaves the second basin to provide the mass conservation. Then, using model (1), the mathematical model for these joined basins reads as follows:

$$\begin{aligned}
\frac{dC^1_{BOD}}{dt} &= A_1 - \left[k^1_1\left(C^1_{DO}\right) + S_1\right]C^1_{BOD} + m^1_1 C^1_{PhT} - \lambda^1 C^1_{BOD} C^1_{DO},\\
\frac{dC^1_{DO}}{dt} &= B_1 + \alpha^1 C^1_{PhT} - \left[k^1_2 + S_1\right]C^1_{DO} - k^1_1\left(C^1_{DO}\right)C^1_{BOD},\\
\frac{dC^1_{PhT}}{dt} &= F_1 + \left[k^1_3\left(C^1_{DO}, C^1_P\right) - m^1\right]C^1_{PhT},\\
\frac{dC^1_P}{dt} &= C_1 - n_1 C^1_{PhT} + n_2 C^1_{BOD} - S_1 C^1_P,
\end{aligned}$$

$$\begin{aligned}
\frac{dC^2_{BOD}}{dt} &= C^1_{BOD}S_2 - \left[k^2_1\left(C^2_{DO}\right) + S_2\right]C^2_{BOD} + m^2_1 C^2_{PhT} - \lambda^2 C^2_{BOD}C^2_{DO},\\
\frac{dC^2_{DO}}{dt} &= C^1_{DO}S_2 + k^2_2 C^{*,2} + \alpha^2 C^2_{PhT} - \left[k^2_2 + S_2\right]C^2_{DO} - k^2_1\left(C^2_{DO}\right)C^2_{BOD},\\
\frac{dC^2_{PhT}}{dt} &= C^1_{PhT}S_2 + \left[k^2_3\left(C^2_{DO}, C^2_P\right) - m^2\right]C^2_{PhT},\\
\frac{dC^2_P}{dt} &= C^1_P S_2 - n^2_1 C^2_{PhT} + n^2_2 C^2_{BOD} - S_2 C^2_P,
\end{aligned} \tag{7}$$

where

$A_1 = \frac{\sum_{j=1}^N q_j c^j_{BOD}}{W_1}$, $B_1 = \frac{\sum_{j=1}^N q_j c^j_{DO}}{W_1} + k^1_2 C^{*,1}$, $F_1 = \frac{\sum_{j=1}^N q_j c^j_{PhT}}{W_1}$, $C_1 = \frac{\sum_{j=1}^N q_j c^j_P}{W_1}$, $S_{1,2} = \frac{\sum_{j=1}^N q_j}{W_{1,2}}$, $k^i_1\left(C^i_{DO}\right) = \frac{k^i_1 C^i_{DO}}{K^i_{DO}+C^i_{DO}}$, $k^i_3\left(C^i_{DO}, C^i_P\right) = k^i_3 \frac{\left(C^i_{DO}\right)^{n^i}}{\left(K^i_v\right)^{n^i}+\left(C^i_{DO}\right)^{n^i}} \cdot \frac{C^i_P}{K^i_\mu + C^i_P}$, $i = 1, 2$.

The system obtained is highly dimensional and nonlinear. Therefore, let's study it by numerical methods. We can assume that all quantities of system (7) are dimensionless (due to application of the procedure mentioned above). Thus, the parameters for the first basin are chosen close to set (6), namely $A_1 = 0.933$, $B_1 = 4.974$, $F_1 = 3$, $C_1 = 2$, $S_1 = 0.2$, $k^1_1 = 1.5$, $k^1_2 = 0.7$, $n^1_1 = 0.65$, $n^2_2 = 0.9$, $k^1_3 = 4.65$, $K_{DO} = 4.3$, $K_v = 0.296$, $K_\mu = 1.14$, $\lambda^1 = 0.7$, $\alpha^1 = 0.05$, $m^1_1 = 0.45$, $m^1 = 2.3$, and the empirical coefficient $n^I = 0.6$.

For the second basin we prescribed the following parameter values $\lambda^2 = 2.3$, $n^{II} = 0.5$, while the rest of parameters are the same as for the first basin. The parameter $C^{*,2}$ characterizing the processes of aeration in the basin is chosen as a control parameter. We start from $C^{*,2} = 1.42$. Omitting the transient processes, system (7) approaches the double periodic regime the phase portrait projection of which is depicted in Fig. 10a. When $C^{*,2} = 1.57$ and $C^{*,2} = 3.4$, the corresponding phase portrait projections are shown in Fig. 10b and c, respectively.

Comparing the amplitude values of the functions from Fig. 10, we can conclude that the increase in oxygen supply in the second basin causes the decrease in the concentration of the nutrient element phosphorus in water. It should be noted that the phosphorus concentration changes quite sharply when the parameter $C^{*,2}$ changes. From the analysis of the phase portraits it also follows that the dynamics of oxygen regime becomes more complex when $C^{*,2}$ increases.

6 Conclusions

Summarizing, we developed the nonlinear mathematical model describing the oxygen regime in water objects. This model is based on the well-known Streeter and Phelps model dealing with the dynamics of BOD and OD. To generalize the Streeter and Phelps model, we incorporate additional factors affecting the oxygen

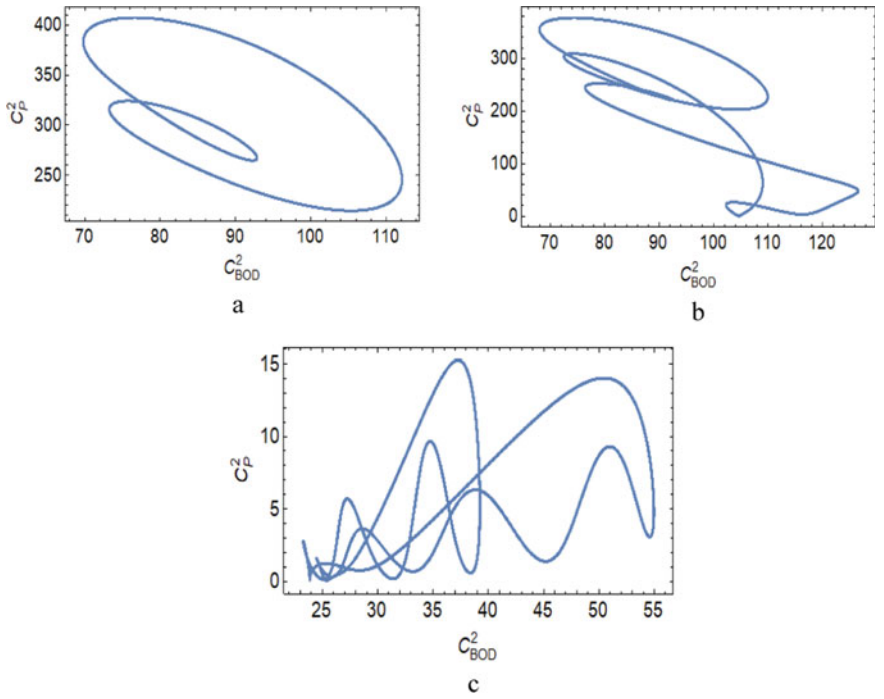

Fig. 10 The phase portraits of system (7) at the following parameters $C^{*,2} = 1.42$ (**a**), $C^{*,2} = 1.57$ (**b**), $C^{*,2} = 3.4$ (**c**)

regime, namely the dynamics of phosphorus and phytoplankton. It should be noted that the study of resulting dynamical system is a complex challenge due to nonlinearity and the high dimension of the system's phase space. Therefore, we apply the qualitative and numerical analysis methods, which provide the information on the model's dynamics without construction of exact system's solutions. We thus shown that model can possess several steady solutions of different stability. The variation of the parameters of nonlinearity causes the change of their stability type, i.e. the bifurcation occurs. In particular, we derived the conditions when the Andronov-Hopf bifurcation takes place. It is shown that due to this bifurcation the nonlinear periodic solution develops. Applying Poincare section technique, we revealed the chain of period doubling bifurcations and the formation of the chaotic attractors. It is worth to note that the revealed attractors represent the limiting states of the system's evolution under the certain set of initial data for the system. Their properties (period, frequency, statistical characteristics, and etc.) are defined by the structure of the system only. This allows one to understand the role of each system's component in the formation of complex dynamical patterns of system's evolution. In other words, these studies shed light on the phenomena of self-organization which emerge in the ecological systems [8, 12, 19, 20].

References

1. Kotsiuba, I.G., Skyba, G.V., Skuratovskaya, I.A., Lyko, S.M.: Ecological monitoring of small water systems: algorithm, software package, the results of application to the Uzh river basin (Ukraine). Methods Objects Chem. Anal. **14**(4), 200–207 (2019)
2. Zabulonov, Y., Popov, O., Burtniak, V., Iatsyshyn, A., Kovach, V., Iatsyshyn, A.: Innovative developments to solve major aspects of environmental and radiation safety of Ukraine. In: Zaporozhets A., Artemchuk V. (eds.) Systems, Decision and Control in Energy II. Studies in Systems, Decision and Control, vol. 346. pp. 273–292 (2021). https://doi.org/10.1007/978-3-030-69189-9_16
3. Zabulonov, Y., Burtnyak., V., Odukalets, L., Alekseeva, O., Petrov, S.: Plasmachemical plant for NPP drain water treatment. Sci. Innov. **14**(6), 86–94 (2018). https://doi.org/10.15407/scine14.06.086
4. Petrovskii, S., Sekerci, Y., Venturino, E.: Regime shifts and ecological catastrophes in a model of plankton-oxygen dynamics under the climate change. J. Theor. Biol. **424**, 91–109 (2017). https://doi.org/10.1016/j.jtbi.2017.04.018
5. Yusta-Garcia, R., Orta-Martinez, M., Mayor, P., Gonzalez-Crespo, C., Rosell-Mele, A.: Water contamination from oil extraction activities in Northern Peruvian Amazonian rivers. Environ. Pollut. **225**, 370–380 (2017). https://doi.org/10.1016/j.envpol.2017.02.063
6. Water Quality Analysis Simulation Program (WASP). Online: https://www.epa.gov/ceam/water-quality-analysis-simulation-program-wasp
7. Leonov, A.V., Pischalnik, V.M.: Modeling of natural processes in water medium. The theoretical foundations. Yuzhno-Sakhalinsk, Sakhalinsk State University, (2012) (in Russian)
8. Yatsyshyn, T., Shkitsa, L., Popov, O., Liakh, M.: Development of mathematical models of gas leakage and its propagation in atmospheric air at an emergency gas well gushing. East. Eur. J. Enterp. Technol. **5/10**(101), 49–59 (2019). https://doi.org/10.15587/1729-4061.2019.179097
9. Zaporozhets, A.O., Redko, O.O., Babak, V.P., Eremenko, V.S., Mokiychuk, V.M.: Method of indirect measurement of oxygen concentration in the air. Naukovyi Visnyk Natsionalnoho Hirnychoho Universytetu **5**, 105–114 (2018). https://doi.org/10.29202/nvngu/2018-5/14
10. Zaporozhets, A., Eremenko, V., Redko, O.: Metrological assessment of the indirect method of measuring the concentration of oxygen in the air. In: 2019 IEEE 8th International Conference on Advanced Optoelectronics and Lasers (CAOL), 640–643 (2019). https://doi.org/10.1109/CAOL46282.2019.9019506
11. Svirizhev, Y.M.: Nonlinear Waves, Dissipative Structures and Catastrophes in Ecology. Nauka, Moscow (1987).(in Russian)
12. Mikhailov, A.S., Loskutov, A.Y.: Foundations of synergetics II: Complex patterns. Springer, Berlin (1991)
13. Lavryk, V.I., Skurativska, I.A.: Mathematical modeling and imitation of the processes of formation and regulation of surface runoff of industrial territories. J. Zhytomyr State Technol. Univ. Eng. **2**(29), 234–239 (2004)
14. Lavryk, V.I., Skurativska, I.A.: Forecasting and control of quality of surface runoff using imitation mathematical modeling. NaUKMA Res. Pap. Biol. Ecol. **29**, 51–57 (2004)
15. Lavryk, V.I., Skurativska, I.A.: Mathematical modeling and estimation of influence of water-gathering area on the oxygen regime of water objects in conditions of their eutrophication, NaUKMA Research Papers. Biol. Ecol. **54**, 46–50 (2006). http://ekmair.ukma.edu.ua/handle/123456789/7877
16. Skurativska, I.A.: Investigation of oxygen regime of water objects in conditions of their eutrophication. NaUKMA Research Papers. Phys. Math. Sci. **51**, 19–24 (2006)
17. Lavryk, V.I., Skurativska, I.A.: Analysis and forecasting of surface drain from industrial regions by means of mathematical and imitation modeling. J. Zhytomyr State Technol. Univ. Eng. **1**(40), 219–225 (2007)
18. Lavryk, V.I., Skurativska, I.A.: The studies of the stability of the oxygen regime of water ecosystems by the methods of mathematical modeling and imitation. Hydrobiol. J. **1**(43), 111–117 (2007)

19. Riznichenko, G.Y.: Mathematical models in biophysics and ecology. Institut of computer researches, Moscow and Izhevsk (2003) (in Russian)
20. Rubin, A., Riznichenko, G.: Mathematical biophysics. Springer, US, (2014)
21. Qinggai, W., Shibei, L., Peng, J., Changjun, Q., Feng, D.: A review of surface water quality models. Sci. World J. Article ID 231768, 7 (2013). https://doi.org/10.1155/2013/231768
22. Dodds, W.K., Whiles, M.R.: Carbon. In: Freshwater Ecology. Concepts and Environmental Applications of Limnology, ch. 13, pp. 323–343. Elsevier, Amsterdam (2010). https://doi.org/10.1016/B978-0-12-374724-2.00013-1
23. Kumar, R., Kumar, A.: Water analysis. Biochemical oxygen demand. In: Worsfold P., Townshend A., Poole C. (eds.) Encyclopedia of analytical science, pp. 315–324. Elsevier (2005)
24. Susilowati, S., Sutrisno, J., Masykuri, M., Maridi, M.: Dynamics and factors that affects DO-BOD concentrations of Madiun River. AIP Conf. Proc. 2049, 020052 (2018). https://doi.org/10.1063/1.5082457
25. Bulai, M.I., Venturino, E.: Two mathematical models for dissolved oxygen in a lake—CMMSE-16. J. Math. Chem. **55**(7), 1481–1504 (2017). https://doi.org/10.1007/s10910-016-0726-4
26. Wang, L.K., Vielkind, D., Wang, M.H.: Mathematical models of dissolved oxygen concentration in fresh water. Ecol. Model. **5**(2), 115–123 (1978). https://doi.org/10.1016/0304-3800(78)90034-0
27. Gotovtsev, A.V.: Modification of the Streeter-Phelps system with the aim to account for the feedback between dissolved oxygen concentration and organic matter oxidation rate. Water Resour. **37**, 245–251 (2010). https://doi.org/10.1134/S0097807810020120
28. Galkin, L.M.: Problems in the construction of mathematical models for self-purificating reservoirs and watercourses. In: Self-Purification and Diffusion on the Internal Reservoirs, pp. 7–47. Novosibirsk (1980)
29. Holzbecher, E.: Environmental Modeling using MATLAB. Springer, Berlin (2012)
30. Holodniok, M., Kliĉ, A., Kubiĉek, M., Marek, M.: Methods of Analysis of Nonlinear Dynamical Models. World Publishing House, Moscow (1991).(in Russian)
31. Zaporozhets, A.O., Khaidurov, V.V: Mathematical models of inverse problems for finding the main characteristics of air pollution sources. Water Air Soil Pollut. **231**, 563 (2020). https://doi.org/10.1007/s11270-020-04933-z
32. Danylenko, V., Skurativskyi, S.: Stationary and periodic regimes in relaxing media with fluctuations. Eur. Phys. J. B **87**, 218 (2014). https://doi.org/10.1140/epjb/e2014-50420-x